PROCEEDINGS OF SPIE

SPIEDigitalLibrary.org/conference-proceedings-of-spie

Interferometric SAR deformation timeseries: a quality index

Wassie, Y., Mirmazloumi, S. Mohammad, Monserrat, O., Crippa, B., Palamà, R., et al.

Y. Wassie, S. Mohammad Mirmazloumi, O. Monserrat, B. Crippa, R. Palamà, A. Barra, M. Crosetto, "Interferometric SAR deformation timeseries: a quality index," Proc. SPIE 11861, Microwave Remote Sensing: Data Processing and Applications, 118610A (12 September 2021); doi: 10.1117/12.2600142

SPIE.

Event: SPIE Remote Sensing, 2021, Online Only

Interferometric SAR deformation timeseries: a quality index

Y. Wassie [1*], S. Mohammad Mirmazloumi[1], O. Monserrat[1], B. Crippa[2], R. Palama[1], A. Barra[1], M. Crosetto[1]

1 Centre Tecnològic de Telecomunicacions de Catalunya (CTTC/CERCA), Division of Geomatics, Av. Gauss, 7 E-08860 Castelldefels, Barcelona (Spain)
2 Department of Earth Sciences, Section of Geophysics, University of Milan, Via Cicognara 7, I-20129, Milan, Italy

ABSTRACT

Estimating unknown absolute phase from a wrapped observation is a challenging and ill-posed problem that possibly leads to misinterpretation of interferometric SAR (InSAR) deformation results. In this study, we introduce a quality index to cluster post-phase unwrapping multi-master InSAR timeseries outputs based on the estimated phase residuals and redundancy of network of interferograms. The index is supposed to indicate the reliability of a timeseries, including the identification of persistent scatterers (PSs) possibly affected by phase unwrapping jumps. The algorithm was tested on two Sentinel-1 interferometric datasets with 622,991 and 95,398 PSs, generated by employing the PSI processing chain, PSIG of the geomatics division of CTTC. Promising result have been achieved–especially in identifying erroneous PSs with phase unwrapping jumps. Along with existing temporal phase consistency checking algorithms, the approach could provide rich information toward a better interpretation of the deformation timeseries results.

Keywords: Data processing, InSAR, Interferometry, phase unwrapping, PSI, Quality index, Time series.

1. INTRODUCTION

Advancements in recent SAR missions with short revisit time boost Persistent Scatterer Interferometry (PSI) processing and analysis methods at high level to a wider range of remote sensing applications. The availability of PSI measurements at all weather conditions and in locations that are inaccessible, remote, or hazardous[1] is also a plus compared to traditional geodetic techniques. Such advantages make the approach more applicable for the monitoring of land subsidence, infrastructures like dams[2], and mining areas to mention few. Since the pioneering work of [3] on PSI has been introduced, a broad and significant development has been made. A critical review in the development of PSI methodologies including main advantages and limitations are discussed in [4,5]. Apart from the wide range of progresses in the past two decades, researches look short on ensuring quality of PSI outputs, time-series of deformation measurements in particular are not seen immune from phase unwrapping effects thus far.

PSI timeseries (TS) methods estimate the spatiotemporal evolution of deformation by incorporating information from multiple SAR interferograms [6]. The principle to generate these dataset lies either on persistent scatterers [3] approach, or on using small baseline interferograms (SB) [7] which is intended for incorporating distributed scatterers (DSs) or based on a technique combining both PSs and DSs [8]. The techniques are mainly devoted to getting quality TS by optimizing several parameters, estimation models and algorithms that builds the whole processing packages. The phase unwrapping step is the crucial one among all TS algorithms to resolve the inherent cycle ambiguities of interferometric phases [9].

*ywassie@cttc.es; phone +34600073498; fax: +34-936-452-901.

Microwave Remote Sensing: Data Processing and Applications, edited by Fabio Bovenga, Claudia Notarnicola, Nazzareno Pierdicca, Emanuele Santi, Proc. of SPIE Vol. 11861, 118610A · © 2021 SPIE · CCC code: 0277-786X/21/$21 · doi: 10.1117/12.2600142

For this, different spatiotemporal approaches have been proposed and implemented [10-12]. Estimating unknown absolute phase from the wrapped observations is challenging and ill-posed. Filtering out PSs affected by phase unwrapping errors is sometimes seen as an alternative remedy to avoid possible misinterpretation of deformation TS results. To alleviate such effects, [13] came up with a robust phase inversion algorithm based on L_1- norm minimization. In 2014, [14] have introduced a technique to characterize quality of time series of PSs based on the ratio of cumulative number of *corrections* in the final iteration of the phase estimation process along with the *redundancy* of interferograms. But, detailed analysis of phase estimation outputs from different case areas signaled the authors of this paper on the necessity of more restrictive approach. This paper is aiming to investigate a supplementary post unwrapping data quality index that make use of phase estimation outputs– residual information at the first iteration and the redundancy of network of interferograms. The index is supposed to indicate the reliability of a TS, including identification of PSs possibly affected by phase unwrapping jumps. The datasets for this study have been generated by using PSIG, the PSI processing chain of the Geomatics division of CTTC. Below, we briefly introduce some of the steps involved in the PSIG chain followed by description of the method and results of the experiment.

2. DATA PROCESSING AND METHODS

In this study, Sentinel-1 SAR datasets– single look complex (SLC) images collected in Interferometric wide swath mode are used. The images are processed burst wise to generate interferograms. For two coregistered SLC images I_1 and I_2, if A_1 and A_2 are the corresponding amplitudes at a point p then the interferogram I_{12} is formed by computing:

$$I_{12} = I_1 I_2^* = A_1 A_2 e^{j\Delta\varphi_{12}} \quad (1)$$

where $\Delta\varphi_{12}$ is the wrapped phase difference of I_1 and I_2 and * is the complex conjugate operator. The wrapped interferometric phase in the direction of a radar line of sight φ_{12}^{los} is modelled as a linear combination of contributions of phase components due to:

- the phase difference resulting from the possible displacement of the target point between image acquisitions, φ_{12}^{defo}
- residual induced topography phase, φ_{12}^{rte}
- the atmospheric phase– variation of medium of propagation of signals between image acquisitions, φ_{12}^{atmo} and
- the phase contribution due to noise, φ_{12}^{noise}

and it is given by:

$$\Delta\varphi_{12}^{los} = \Delta\varphi_{12}^{defo} + \Delta\varphi_{12}^{atmo} + \Delta\varphi_{12}^{rte} + \Delta\varphi_{12}^{noise} \quad (2)$$

The goal is to reconstruct $\Delta\varphi_{12}^{defo}$ from observations $\Delta\varphi_{12}^{los}$ and other phase components including those estimated and/or compensated from external datasets like DEMs and orbit files. Swath and burst selection and extraction, co-registration of selected bursts, geometric calibration of super master and the digital elevation model followed by interferogram network formation, generation of interferograms, merging of interferograms and generation of mean amplitude and dispersion of amplitude images are the main steps implemented in the first block of the processing chain. Though not in the scope of this study, residual topographic phase estimation and spatio-temporal filtering algorithms are also involved in the retrieval of deformation phases, $\Delta\varphi_{12}^{defo}$. While the first one is intended for the reconstruction of differential residual topographic errors (rte) from network of selected PSs, the latter one is dedicated to separate the atmospheric signals (atmo) from deformation signals by spatial low pass filtering and temporal high pass filtering algorithms. Some of the main processing tools are briefly discussed as follows.

2.1 Point selection

This is the procedure implemented to select target points that reflect signals to radar sensors persistently in time, called persistent scatterers. Buildings, metallic structures and exposed rocks are some of the features showing these

characteristics[15]. Corner reflectors have also played a significant role in serving as a PS mainly in rural areas [16,17]. Points with significant decorrelation effects are discarded at this step. The criteria of dispersion of amplitudes or coherence-based criteria are mainly used for this purpose. The threshold used in either criterion is a tradeoff between quality and density of points that also highly influence quality of results in the upcoming processes. The dispersion of amplitude which is the measure of phase stability is given by [3]:

$$D_A = \frac{\sigma_A}{\mu_A} \tag{3}$$

where σ_A and μ_A respectively refer to the standard deviation and mean amplitude of the images used in the processing. The spatial phase coherence is also an alternative approach used for point selection. Given zero mean complex signal pairs z_M and z_S of image M and S, the coherence of the corresponding interferogram at point $\mathfrak{p}$ is estimated from neighboring pixels $\mathfrak{p}_i$ within a window Ω by [18]:

$$\hat{\gamma}_{\mathfrak{p}} = \frac{\left|\sum_{\mathfrak{p}_i \epsilon \Omega} z_M(\mathfrak{p}_i) z_S^*(\mathfrak{p}_i)\right|}{\left(\sum_{\mathfrak{p}_i \epsilon \Omega} |z_M(\mathfrak{p}_i)|^2 \sum_{P_i \epsilon \Omega} |z_S(\mathfrak{p}_i)|^2\right)^{\frac{1}{2}}} \tag{4}$$

where $*$ stands for the complex conjugate operator, and Ω is the set of pixels in the neighborhood of $\mathfrak{p}$.

2.2 Phase unwrapping

At this stage the absolute differential interferometric phases are reconstructed by adding integer multiples of 2π to the wrapped differential phases Eq.(5). Unwrapped phase, ψ is related to its wrapped counterpart, φ by the modulo operator as:

$$\varphi = \psi \bmod 2\pi \Leftrightarrow \psi = \varphi + 2k\pi \tag{5}$$

where the unknown $k \in \mathbb{Z}$ is to be estimated. This represents a critical and error-prone processing stage. The errors could be attributed to phase noise, high deformation rates or isolated pixels when neighboring pixels are too far apart. The phase unwrapping algorithm in the PSIG chain involves a spatial 2D phase unwrapping using a Minimum Cost Flow method[10] followed by a temporal 1D phase estimation procedure. This estimation is done point wise exploiting the temporal evolution of each point of the SAR images and intended to detect and correct errors generated, if any, in the 2D phase unwrapping [19].

2.3 Phase estimation

Let $\hat{\boldsymbol{\varphi}}$ denotes the estimate of n unknown phases in the LOS direction and let $\boldsymbol{\psi}$ be the vector of known phases of m differential interferograms. The estimation of TS of phases from unwrapped interferograms is formulated from the model:

$$D.\hat{\boldsymbol{\varphi}} = \boldsymbol{\psi} \tag{6}$$

D is a known design matrix each of whose rows contain -1, 0 and 1. In a fully connected network, $\hat{\boldsymbol{\varphi}}$ can be estimated by solving Eq.(7) for an associated weight matrix $\boldsymbol{w}$. Otherwise, singular value decomposition (SVD) technique would be used in estimating the minimum norm or least square solution of the system of equation in Eq. (6).

$$\hat{\boldsymbol{\varphi}} = (D^T \boldsymbol{w} D)^{-1} D^T \boldsymbol{w} \boldsymbol{\psi} \tag{7}$$

More detail information on SVD decomposition is available in [7,20,21]. In the PSIG chain, the phase estimation procedure is accompanied by outlier correction/rejection criterion and are briefly described in Fig.1.

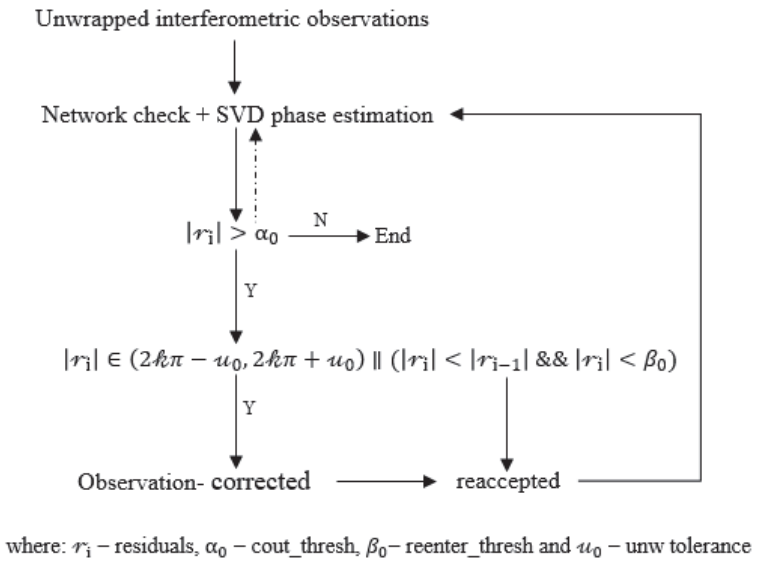

Figure 1. Phase estimation flow chart.

The procedure is executed iteratively for each observation until there are no remaining outlier candidates–observations where $|r_i| > \alpha_0$. For unwrapping tolerance, u_0 if an error lies within $2k\pi \pm u_0$, then it will be corrected. Besides, a candidate outlier will be reaccepted to the network if its residue in upcoming estimations– is below β_0 otherwise will be rejected [14]. The phase estimation procedures improve the result drastically. For instance, from the Barcelona dataset, the standard deviation of residuals of a PS improved from 6.22 rad in the first iteration to 0.74 rad in the final iteration, see Fig.2(a). On the other hand, a possible phase unwrapping effect has also been observed for some of the cases–like the jump shown in Fig.2(b). After an extensive experiment, we found that abrupt change in the amplitude data is one of the causes for such errors. Thus, identifying PSs of this type is a crucial post unwrapping step and will clearly augment interpretation of deformation TSs.

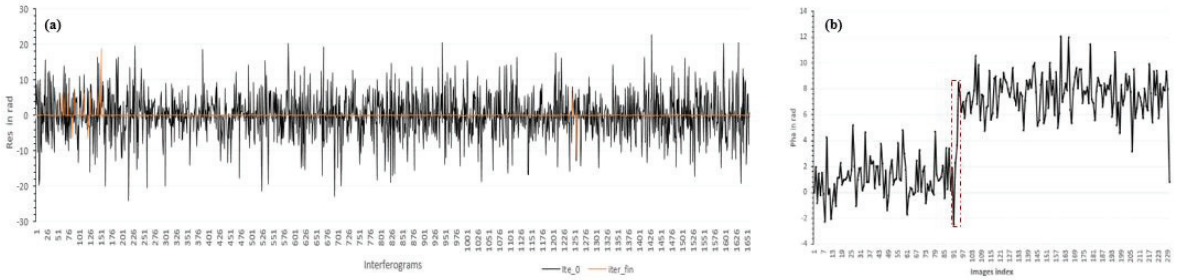

Figure 2. Phase estimation sample outputs: (a) residuals at the first (black colored signal) and final (orange colored signal) iterations and (b) estimated phase with unwrapping jump.

2.4 TS index

Labeling of deformation TS information could facilitate interpretation of results. In this study, a three-class quality index indicating reliability of PSs was introduced. For each PS p, we defined a real valued function ξ, as formulated in Eq.(10), that make use of the residuals and redundancy of network of interferograms to highlight their reliability. The values of the function were used to classify PSs into classes– identified as *more reliable* (C1), *reliable* (C2) and *less reliable* (C3). The PSs were assigned in either of these classes in the following way.

For a residual r_{ij} of point $\mathfrak{p}_{ij}$, determined in the phase estimation, we define

$$\mathfrak{B}_{\mathfrak{p}_{ij}} = \begin{cases} 1, & \text{if } |r_{ij}| > \alpha_0 \\ 0, & \text{otherwise} \end{cases} \tag{8}$$

and let,

$$\mathfrak{B}_{\mathfrak{p}_i} = \frac{\sum_j^{k_i} \mathfrak{B}_{\mathfrak{p}_{ij}}}{k_i}, \text{ for } 1 \le j \le k_i. \tag{9}$$

where k_i stands for the redundancy corresponding to image i.

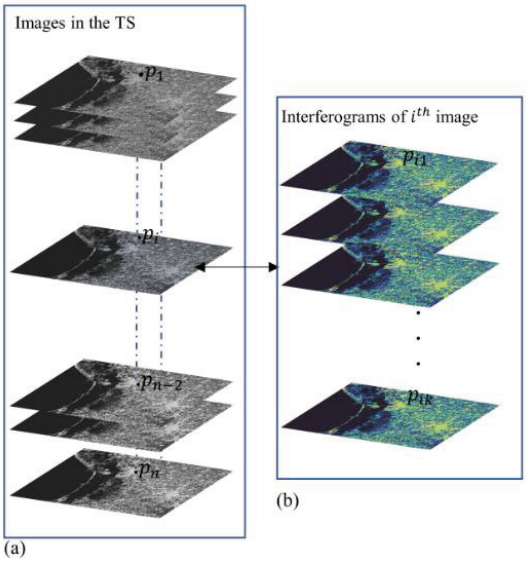

Figure 3. Stack of (a) SLC images in the TS & (b) unwrapped interferograms associated to i[th] image

Then, for each $\mathfrak{p}$ in the TS, $\xi(\mathfrak{p})$ is computed as;

$$\xi(\mathfrak{p}) = \frac{1}{n}\sum_{i=1}^{n} \mathfrak{B}_{\mathfrak{p}_i} = \frac{1}{n}\sum_{i=1}^{n} \frac{1}{k_i}\sum_{j=1}^{k_i} \mathfrak{B}_{\mathfrak{p}_{ij}} \tag{10}$$

and the PSs were then assigned to the classes as per the following criterion:

$$\begin{cases} \mathfrak{p} \in C_3 \text{ if } \xi(\mathfrak{p}) \ge q_3 \\ \mathfrak{p} \in C_2 \text{ if } q_1 < \xi(\mathfrak{p}) < q_3 \\ \mathfrak{p} \in C_1 \text{ if } \xi(\mathfrak{p}) \le q_1 \end{cases} \tag{11}$$

where q_1 and q_3 are, respectively, the first and third quartiles in the distribution of $\xi(\mathfrak{p})$ and n is the number of images in the TS. The value of ξ ranges between 0 and 1 inclusive and the more it gets closer to 1, the more erroneous the corresponding PS would be. Ratio of number of nonzero $\mathfrak{B}_{\mathfrak{p}_i}$ to the total number of images in the TS was also used as a measure to classify PSs along with Eq.(11). The idea is thus to classify all values of $\xi(\mathfrak{p})$ into three classes quantifying the reliability of the PSs based on median based threshold. Apart from the procedures, its indirect nature makes it unique from approaches identified in literature.

3. RESULTS

We tested the algorithm on Barcelona dataset involving 622,991 TSs generated from 230 Sentinel-1 SLC images covering the period from 2016 to 2021 (1657 interferograms, 2 swaths, 2 bursts). To see the response of the algorithm for different datasets, 95,398 PSs selected from 57 Sentinel-1 SLC images (321 interferograms, a portion of a burst) were also used from Poland datasets. Results of Poland and Barcelona datasets are summarized in Fig.4 and Fig.5, respectively.

The plots in Fig.4 highlight the success of the algorithm in clustering similar TSs in the same group. The mean standard deviations of TSs in the subplots (a), (b) and (c) are, respectively, computed as 0.84, 1.92 and 2.88 rad. TSs from different classes are also plotted together in subplot (d) to ease the comparison.

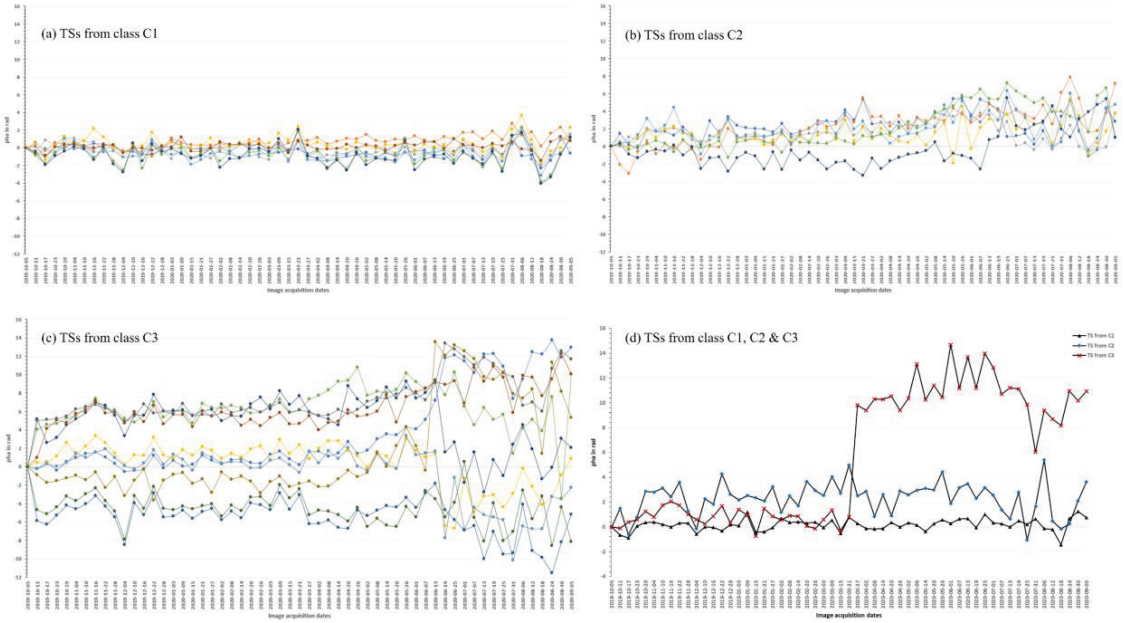

Figure 4. Sample TSs from Poland datasets: TSs from the same class plotted in sublots (a) to (c) and TSs from different classes plotted on the same subplot (d).

We have noticed that PSs with possible unwrapping error are categorized in the less reliable class (C3). In subplot (d) of Fig.4, for instance, the TS that belongs to class C3 depicts a phase jump from 0.78 rad to 9.805 rad from date 21-03-2020 to 27-03-2020. It is also important to note that in very few instances the index wasn't found reflecting the real behavior of phase information. This could possibly result from the residual threshold used to identify candidate outliers, and from the indirect nature of the quality index algorithm itself.

Generally, as in the results from the Poland datasets, more erroneous PSs of the Barcelona datasets were clustered in class–C3. To justify this, we plotted three TSs from C1, C2 and C3 in Fig. 5(b). From which the standard deviations of lime green (from C2) and dark green (from C1) TSs are found to be 1.84 and 0.92 rad, respectively. Whereas, the standard deviation of the dark red TS, which belongs to C3, is 2.30 rad. In relation to the Poland datasets, one notable difference we observed is– in the Barcelona dataset more PSs at the far range position are categorized in the less reliable class (C3) as shown in Fig.5(a). The distribution of ξ used to define the thresholds in the clustering of the Barcelona dataset is presented in Fig.5(c).

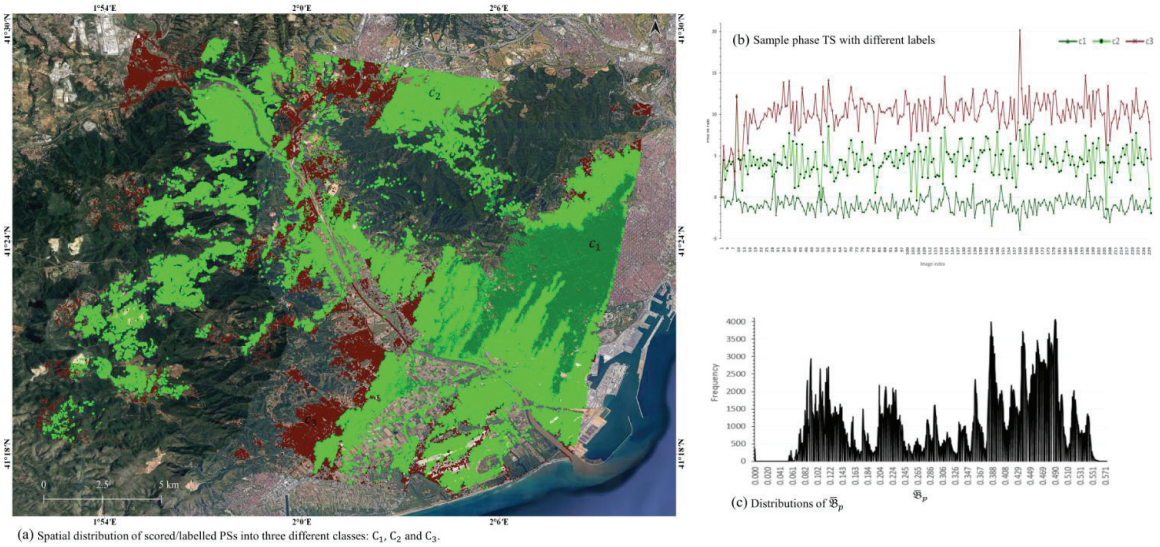

Figure 5. Outputs from Barcelona datasets: (a) Spatial distribution of 622991 PSs clustered to the three classes: C1–in dark green (also contains the reference point), C2–lime green and C3–dark red, (b) sample TSs taken from these classes–colors of the TS correspond to the respective classes (c) distribution of values of $\bar{\xi}$ at each PS.

The result also justified that PSs closer to a reference point are more reliable.

4. CONCLUSION

This study proposes a quality index to cluster post phase unwrapping InSAR TS outputs. The index was calculated based on the estimated phase residuals and redundancy of network of interferograms. This makes the approach suitable only for multi-master small baseline InSAR TS deformation analysis techniques. The algorithm was tested on different datasets with 622,991 and 95,398 TS of PSs generated from Sentinel-1 SLC images. The set of PSs in each of the datasets were assigned to three classes– that are supposed to indicate their reliability. Generally, a promising result have been achieved–including clustering of PSs with phase unwrapping jumps into the less reliable class. The importance of estimated phase residuals and redundancy of network of interferograms in assisting the interpretation of the final deformation TS has been justified. The contributions of the approach for PS quality improvement from the perspectives of outlier detection and data reduction are to be further investigated.

ACKNOWLEDGEMENT

This work has been funded by AGUAR, Generalitat de Catalunya, in the framework of Resolution EMC/ 2459/2019, FI-2020.

REFERENCES

[1] Parker, A. L., [InSAR Observations of Ground Deformation], Springer International Publishing, Cham (2017).

[2] Di Martire, D., Iglesias, R., Monells, D., Centolanza, G., Sica, S., Ramondini, M., Pagano, L., Mallorquí, J. J. and Calcaterra, D., "Comparison between Differential SAR interferometry and ground measurements data in the displacement monitoring of the earth-dam of Conza della Campania (Italy)," Remote Sens. Environ. **148**, 58–69 (2014).

[3] Ferretti, A., Prati, C. and Rocca, F., "Permanent scatterers in SAR interferometry," IEEE Trans. Geosci. Remote Sens. **39**(1), 8–20 (2001).

[4] Crosetto, M., Monserrat, O., Cuevas-González, M., Devanthéry, N. and Crippa, B., "Persistent Scatterer Interferometry: A review," ISPRS J. Photogramm. Remote Sens. **115**, 78–89 (2016).

[5] Pepe, A. and Calò, F., "A Review of Interferometric Synthetic Aperture RADAR (InSAR) Multi-Track Approaches for the Retrieval of Earth's Surface Displacements," Appl. Sci. **7**(12), 1264 (2017).

[6] Shanker, P., Casu, F., Zebker, H. A. and Lanari, R., "Comparison of Persistent Scatterers and Small Baseline Time-Series InSAR Results: A Case Study of the San Francisco Bay Area," IEEE Geosci. Remote Sens. Lett. **8**(4), 592–596 (2011).

[7] Berardino, P., Fornaro, G., Lanari, R. and Sansosti, E., "A new algorithm for surface deformation monitoring based on small baseline differential SAR interferograms," IEEE Trans. Geosci. Remote Sens. **40**(11), 2375–2383 (2002).

[8] Ferretti, A., Fumagalli, A., Novali, F., Prati, C., Rocca, F. and Rucci, A., "A New Algorithm for Processing Interferometric Data-Stacks: SqueeSAR," IEEE Trans. Geosci. Remote Sens. **49**(9), 3460–3470 (2011).

[9] Ajourlou, P., Samiei Esfahany, S. and Safari, A., "A new strategy for phase unwrapping in insar time series over areas with high deformation rate: Case study on the southern tehran subsidence," Int. Arch. Photogramm. Remote Sens. Spat. Inf. Sci. - ISPRS Arch. **42**(4/W18), 35–40 (2019).

[10] Costantini, M., Farina, A. and Zirilli, F., "A fast phase unwrapping algorithm for SAR interferometry," IEEE Trans. Geosci. Remote Sens. **37**(1), 452–460 (1999).

[11] Chen, C. W. and Zebker, H. A., "Two-dimensional phase unwrapping with use of statistical models for cost functions in nonlinear optimization," J. Opt. Soc. Am. A **18**(2), 338 (2001).

[12] Li, W., Zhao, C., Wang, B. and Zhang, Q., "L^1-Norm Sparse 2-D Phase Unwrapping Algorithm Based on Reliable Redundant Network," IEEE Geosci. Remote Sens. Lett.(February 2021), 1–5 (2021).

[13] Lauknes, T. R., Zebker, H. A. and Larsen, Y., "InSAR Deformation Time Series Using an L_{1}-Norm Small-Baseline Approach," IEEE Trans. Geosci. Remote Sens. **49**(1), 536–546 (2011).

[14] Devanthéry, N., Crosetto, M., Monserrat, O., Cuevas-González, M. and Crippa, B., "An Approach to Persistent Scatterer Interferometry," Remote Sens. **6**(7), 6662–6679 (2014).

[15] Crosetto, M., Monserrat, O., Cuevas, M. and Crippa, B., "Spaceborne Differential SAR Interferometry: Data Analysis Tools for Deformation Measurement," Remote Sens. **3**(2), 305–318 (2011).

[16] Crosetto, M., Luzi, G., Monserrat, O., Barra, A., Cuevas-González, M., Palamá, R., Krishnakumar, V., Wassie, Y., Mirmazloumi, S. M., Espín-López, P. and Crippa, B., "Deformation monitoring using SAR interferometry and active and passive reflectors," Int. Arch. Photogramm. Remote Sens. Spat. Inf. Sci. **XLIII-B3-2**, 287–292 (2020).

[17] Luzi, G., Espín-López, P. F., Pérez, F. M., Monserrat, O. and Crosetto, M., "A low-cost active reflector for

interferometric monitoring based on sentinel-1 sar images," Sensors **21**(6), 1–21 (2021).

[18] Touzi, R., Lopes, A., Bruniquel, J. and Vachon, P. W., "Coherence estimation for SAR imagery," IEEE Trans. Geosci. Remote Sens. **37**(1), 135–149 (1999).

[19] Pepe, A. and Lanari, R., "On the Extension of the Minimum Cost Flow Algorithm for Phase Unwrapping of Multitemporal Differential SAR Interferograms," IEEE Trans. Geosci. Remote Sens. **44**(9), 2374–2383 (2006).

[20] Golub, G. H. and Van Loan, C. F., [Matrix Computations., 4th ed.], JHU Press, Baltimore, Maryland, USA (2013).

[21] Tao, Q., Ding, L., Hu, L., Chen, Y. and Liu, T., "The performance of LS and SVD methods for SBAS InSAR deformation model solutions," Int. J. Remote Sens. **41**(22), 8547–8572 (2020).